Technical Report No. 41

HIGH FLOWS IN THE 21ST CENTURY: ANALYSIS WITH A SIMPLE CONCEPTUAL HYDROLOGICAL MODEL USING THE INPUT OF 3 GCMS (A2 SCENARIO)

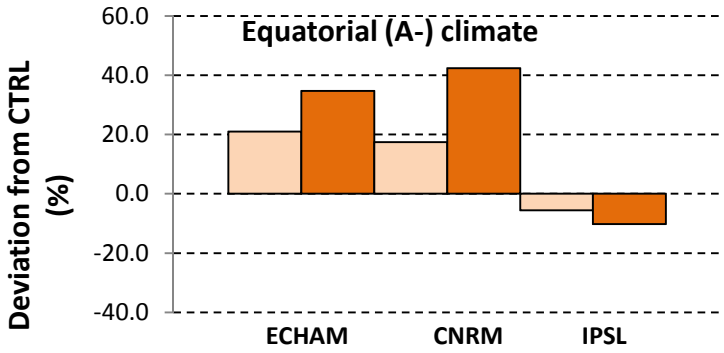

Henny A.J. van Lanen & Niko Wanders

25 August 2011

WATCH is an Integrated Project Funded by the European Commission under the Sixth Framework Programme, Global Change and Ecosystems Thematic Priority Area (contract number: 036946).
The WACH project started 01/02/2007 and will continue for 4 years.

Title:	High flow in the 21st Century: analysis with a simple conceptual hydrological model using the input of 3 GCMs (A2 scenario).
Authors:	Henny A.J. van Lanen & Niko Wanders
Organisations:	- Wageningen University - Hydrology and Quantitative Water Management Group (WUR), Wageningen, the Netherlands - Utrecht University, Department of Physical Geography, Faculty of Geosciences, Utrecht, the Netherlands
Submission date:	25 August 2011
Function:	This report is an output from Work Block 4; Task 4.3.2 Frequency, severity and extent of floods in 21st century.
Deliverable	WATCH deliverables D 4.3.1b Assessment of the future change in major large-scale floods and their main physical aspects (likely frequency, severity, extent), including an assessment of the uncertainty and D 4.3.2 Report on the sensitivity of future droughts and large-scale floods for climate change, and it contributes to M4.3-2 Future change of large-scale flood.

Photo cover: Left: Large-scale flooding (River Rhine near Wageningen)
Right: Impact of climate change on high flows in the near future (lighter colour) and end of the 21st century (darker colour) according to three GCMs.

Table of Contents

1. Introduction

Flooding is a natural hazard that occurs everywhere across the globe. Over the last decades, various regions in the world were hit hard by large-scale floods (e.g. Pakistan, East Australia, Bangladesh, New Orleans, Central Europe). Floods are complex phenomena involving numerous interacting weather processes and various land processes (e.g. antecedent river basin wetness). Floods have large socio-economic and environmental impacts affecting many sectors (e.g. EEA, 2010). Some floods also cause many fatalities. Different types of flooding can be distinguished, e.g. flash floods, river floods, coastal surges. Likely the scale, frequency and severity of flooding will increase due to climate change (e.g. IPCC 2007a: 2007b; 2007c; EEA, 2007; 2008; UN-ISDR, 2009; Bates *et al*., 2009). Hence, there is an urgent need to improve flood preparedness through measures that reduce vulnerability and the risks floods pose world-wide, in particular considering the uncertain future.

The WATCH project focused on large-scale river floods. Within the project hydrological extremes, incl. large-scale floods, are investigated through the analysis of the outcome from a set of large-scale models (i.e. multi-model experiments) (Haddeland *et al*., 2011). Some of these so-called WaterMIP models are classified as global hydrological models (GHMs), whereas others belong to the off-line land surface models (LSMs). All models were run over the period 1963-2001 on a global 0.5 degree grid and forced by the same weather data obtained from new re-analysis dataset, i.e. WATCH Forcing Data (WFD, Weedon *et al*., 2011). Prudhomme *et al.* (2011) explored to what level three of the WaterMIP large-scale models are able to simulate daily high flows as a proxy for floods in Europe. Some systematic weaknesses emerge in all models, which could be a product of poor spatial resolution of the input climate data (e.g. where extreme precipitation is driven by local convective storms) or topography. Gudmundsson *et al.* (2011) used a larger set of WaterMIP models and uncovered that most large-scale models over-estimate monthly high flows. Stahl *et al.* (2011) compared trends in annual and monthly simulated flow from eight WaterMIP models against observations in Europe and found rather large differences among the models and the best agreement for the multi-model ensemble mean. Most of the WaterMIP models have also been run for the 21st Century and for a control period (CTRL, 1960-2000). Downscaled, bias-corrected climate data from a number of General Circulation Models (GCMs) for a couple emission scenarios has been used as input (Chen *et al*., 2011). Future high flows will also be investigated using the outcome of these models (Fig. 1.1).

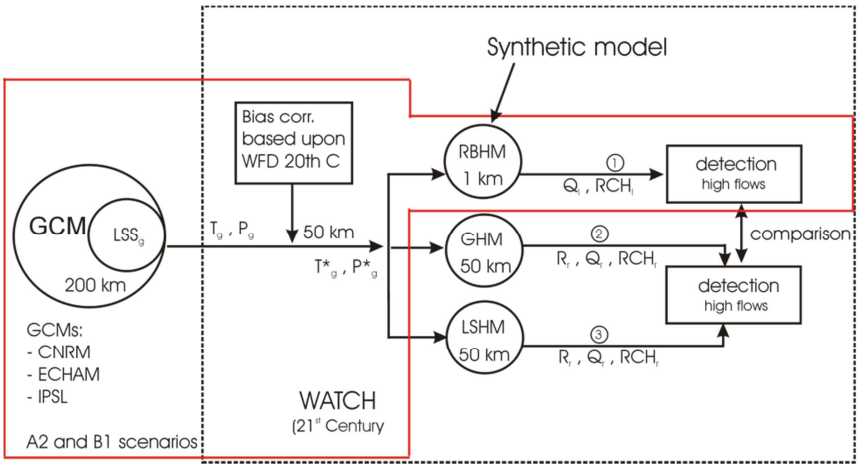

Figure 1.1 Flow chart showing the context of the assessment of high flows for the 21st Century within WATCH.

Figure 1.1 shows that within WATCH, the outcome from three GCMs has been bias corrected and fed into a set of WaterMIP large-scale models (GHMs and LSMs). Time series of these models have been used: (i) to assess future flood peaks for (Miller *et al*., 2011), and (ii) to project changes in future runoff

variability (Gudmundsson *et al*., 2011). Both studies cover Europe. It was beyond the scope of the WATCH project to perform similar studies with the WaterMIP large-scale models (GHMs and LSMs) on high flows for the whole globe. As an alternative and a first step a simple conceptual hydrological model has been used to explore future high flows. This model will support interpretation of the model outcome from GHMs and LSMs in the next phase.

The aim of this study is: (i) to check high flows obtained with the hydrological model using the three GCMs against those got from the re-analysis dataset (WATCH Forcing Data) for the control period (CTRL, 1970-2000), and (ii) to explore future high flows for the periods 2021-2050 and 2071-2100 obtained with the three GCMs and for the A2 scenario.

First we will provide an overview of the approach, summarize the main properties of the conceptual hydrological model that has been used in this study followed by a description of the common forcing data (three GCMs, i.e. CRNM, ECHAM, IPSL), the high flow identification approach and the data used (Chapter 2). Then we will explore for the control period (1971-2000) whether the hydrological model fed by climate forcing of three GCMs (i.e. CRNM, ECHAM, IPSL) can reproduce the drought derived from the same model, but then forced by WFD (reanalysis data). Next we will describe global future drought (Chapter 3). Finally, we will draw some conclusions.

2. Methods and Materials

This chapter starts with an overview of the approach that is followed by a brief description of the conceptual hydrological model followed, an explanation of the common forcing data (three GCMs, i.e. CRNM, ECHAM, IPSL) and the high flow identification approach. The chapter concludes with the data used for the modelling and high flow identification.

2.1. Approach

2.1.1. Overview

Time series of climate data from a global re-analysis dataset have been used as driving force for a conceptual hydrological model that combines a soil water balance model and simple spatially-lumped groundwater model (e.g. Van Lanen *et al.*, 2011). Four time series of global climate data have been used for this study on high flows:

- re-analysis dataset (WATCH Forcing Data, WFD), 1971-2000;
- GCM data from CNRM, 1970-2100;
- GCM data from ECHAM, 1970-2100;
- GCM data from IPSL, 1970-2100.

The conceptual model has been run for these four climate times series and a vast number of randomly selected land grids across the globe assuring that the different global climates are well represented (Figure 2.1). The adopted approach does not generate a time series of hydrometeorological variables that consider the unique site conditions of a specific land grid at the globe as Global Hydrological Models (GHMs) or Land Surface Models (LSMs) do, rather it produces a possible time series of hydrometeorological variables (i.e. a single realization) for that land grid for a reference physical catchment structure. The discharge is one of the hydrometeorological variables.

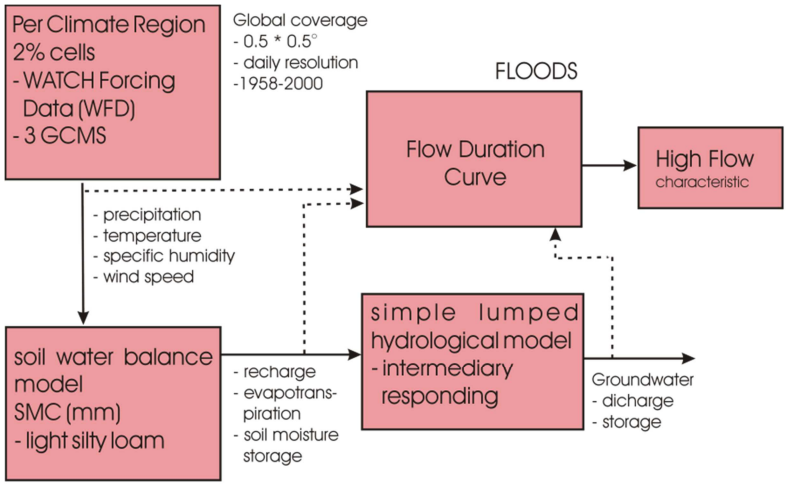

Figure 2.1 Flow chart showing the overall procedure.

We used the time series of the discharge for the computation of flow duration curve (FDC), which was the basis for the determination of the high flow characteristic. Three different periods were distinguished:

- Control period (CTRL), 1971-2000;
- Intermediate future, 2021-2050;
- End of century, 2071-2100

The period 1971-2000 was distinguished to compare the high flow characteristic that was computed from the simulated discharge with the re-analysis climate data with the characteristic we obtained for each of the three GCMs. The other two periods in the 21st Century provide information about possible changes because of climate change. The results are presented for the five Köppen-Geiger major climate regions.

2.1.2. Conceptual hydrological model

Soil water balance model

A transient soil-water balance model (Fig. 2.2) that uses daily precipitation, temperature and reference evaporation as forcing data was applied to simulate time series of daily snow melt, snow storage, actual evapotranspiration, soil moisture storage and groundwater recharge (Van Lanen *et al*., 1996; 2011). Land use and soil data characterize the physical catchment structure. The model solves the following daily water balance equations:

$$SS_t = SS_{t-1} + Pra_t + Qsn_t - ETa_t - Rch_t \quad (1)$$

$$Sn_t = Sn_{t-1} + Psn_t - Qsn_t \quad (2)$$

$$Rch_t = Qs_t + Qb_t \quad (3)$$

where: *SS* is soil water storage (mm), *Pra* is rainfall (mm day^{-1}), *Qsn* is snow melt (mm day^{-1}), *ETa* is actual evapotranspiration (mm day^{-1}), *Rch* is groundwater recharge (mm day^{-1}), *Sn* is snow storage (mm), *Psn* is snow fall (mm day^{-1}), *Qs* is downward flux across the bottom of the soil (mm day^{-1}), *Qb* is bypass flow, i.e. part of rainfall that bypasses the soil (mm day^{-1}), and *t* denotes time (day).

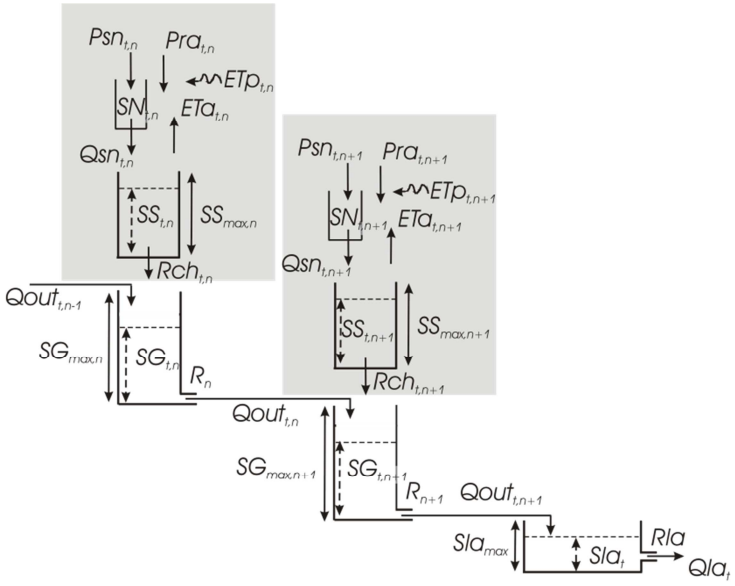

Figure 2.2 Conceptual diagram of hydrological model.

The model uses the approach of the well-known hydrological model HBV to simulate snow accumulation and snow melt (Seibert, 2005). Accumulation of precipitation as snow takes place if temperature is lower than a threshold temperature *TT*, which normally is close to 0°C. Melt of snow (Qsn_t) starts if daily

temperature $T_t > TT$. It is calculated with a degree-day method, i.e. the daily temperature difference (T_t - TT) is multiplied by a parameter $CFMAX$ (mm $^oC^{-1}$ day^{-1}). All precipitation that is simulated to be snow is multiplied by a correction factor, $SFCF$, to account for snow losses (e.g. sublimation) and undercatch due to wind effects. The snow pack retains melt water until the amount exceeds a certain threshold (CWH, fraction of the water equivalent of the snow pack). When the temperature T_t decreases below TT melt water in the snow pack refreezes, which is controlled by the parameter CFR and the temperature difference (TT-T_t).

Potential evapotranspiration (ETp_t, mm day^{-1}) is computed by multiplying daily reference evaporation (ET_o, mm day^{-1}) and time-dependent crop factors (Allen *et al.*, 1998). Crops transpire at a potential rate as long as SS_t is between field capacity (SS_{FC}) and critical soil moisture storage (SS_{CR}), implying that $ETa_t = ETp_t$. For dryer conditions ETa_t is smaller than ETp_t and it is calculated by multiplying ETp_t with the factor (SS_t - SS_{WP}) / (SS_{CR} - SS_{WP}), where: SS_{WP} is soil moisture storage at wilting point. ETa_t=0 when the soil is dryer than wilting point.

The downward flux across the bottom of the soil (Qs_t) is simulated as follows:

$$\begin{aligned} Qs_t &= SS_t - SS_{FC} && if\ SS_t > SS_{FC} \\ Qs_t &= \left(\frac{SS_t - SS_{CR}}{SS_{FC} - SS_{CR}} \right)^b * k_{FC} && if\ SS_{CR} < SS_t < SS_{FC} \\ Qs_t &= 0 && if\ SS_t < SS_{CR} \end{aligned} \qquad (4)$$

where: k_{FC} is unsaturated hydraulic conductivity at field capacity (mm day^{-1}) and b (-) is a shape parameter that is derived from the soil moisture retention and the unsaturated hydraulic conductivity curve.

The approach has similarity with HBV that also simulates recharge for soils dryer than field capacity (Seibert, 2005). Additionally, rainfall bypassing the soil and directly feeding the groundwater system (Qb_t) occurs in dry clay-rich soils (e.g. Van Stiphout *et al.* 1987, Bronswijk, 1988). In this study we assumed that Qb_t takes place if $SS_t < SS_{CR}$ and it equals a fraction of the rainfall.

Groundwater model

A lumped groundwater model that is based upon linear reservoir theory has been applied to simulate time series of groundwater discharge into a stream. The simulated time series of groundwater recharge (Rch_t) are used as driving force for the groundwater model (Van Lanen *et al.*, 2004). The groundwater model uses the De Zeeuw-Hellinga approach (Kraijenhof van de Leur, 1962; Ritsema, 1994):

$$Qout_t = Qout_{t-1} * e^{-1/j} + Rch_t * (1 - e^{-1/j}) \qquad (5)$$

where: $Qout$ is groundwater discharge (mm day^{-1}), and j is a response parameter (day).

For naturally drained aquifers, a general interpretation for the response parameter is (Birtles and Wilkinson, 1975):

$$j = \frac{\mu * L^2}{kD} \qquad (6)$$

where: kD is transmissivity of the groundwater system ($m^2\ day^{-1}$), μ is storage coefficient of the groundwater system (-), and L is distance between streams (m). These three parameters allow calculation of response parameters that reflect particular groundwater systems (e.g. quickly responding, slowly responding). Readers are for more details referred to Van Lanen *et al*. (2011).

2.1.3. Future climate

The output from three coupled atmosphere/ocean GCMs for the A2 emission scenario was considered in the present study (Hagemann et al., 2011). These include ECHAM5, CNRM and IPSL (Table 2.1).

Table 2.1 Three IPCC AR4 GCMs and their spatial resolution

Centre	GCM	Horizontal resolution	Vertical resolution
MPI-M	ECHAM5/MPIOM T63	~ 1.9°~ 200 km	L31
CNRM	CNRM-CM3 T42	~ 2.8°~ 300 km	L45
IPSL	LMDZ-4	3.75°x 2.5°~ 300 km	L19

For each GCM, a present day control period from 1960-1999 was used to derive the parameters necessary for the bias correction (Piani *et al.*, 2010a; 2010b). The GCM data were bias corrected with data from the WATCH Forcing Dataset (WFD). WFD is a re-analysis dataset. For more details readers are referred to Weedon *et al.* (2010; 2011).

Then, the bias correction was applied to the control period as well as to the A2 scenario for the period 2000-2100 (Hagemann *et al.*, 2011). In WATCH total precipitation was corrected using transfer functions, and snowfall was corrected accordingly using the snowfall fraction taken from the GCM. In addition, mean (Tmean), minimum (Tmin) and maximum (Tmax) daily temperatures were also corrected. It should be pointed out that the bias correction also includes statistical downscaling of the GCM outcome to 0.5°, which is due to the higher resolution of the WFD of 0.5° as compared to the GCM resolutions (see Table 2.1). This means that first, the GCM data were interpolated to 0.5° resolution, and then they were bias corrected at 0.5° with the WFD. Especially in regions with large orographic gradients, the higher resolution contains features not present in the low resolution GCM data, such as orographic precipitation. Note that the accuracy of the bias correction is always limited by the quality of the observational data used. Consequently, bias corrected GCM data may be less reliable in data sparse regions.

2.1.4. Identification of high flow

High flow was derived from the simulated time series of daily groundwater discharge ($Qout_t$) by using the threshold level approach (Yevjevich, 1967; Prudhomme *et al.*, 2011). The threshold level for discharge (Q10) was derived from the flow duration curve (i.e. the 10% percentile). The Q10 is equalled

or exceeded in 10% of the time. The varying threshold level that regularly is used in drought studies (e.g. Hisdal et al., 2004; Van Lanen & Tallaksen, 2007) has been used to cope with a marked seasonality and is also chosen for this high flow study. A monthly-varying threshold level was used, implying that the 10% percentile from all daily data for a certain month were analyzed to identify the 12 different thresholds (Q10(i)). The discrete monthly threshold values were smoothed by applying a centered moving average of 30 days to avoid problems by only using the discontinuous curve with the 12 monthly thresholds (Van Loon et al., 2010).

2.2. Data

Hydroclimatic data

Hydroclimatic data in this study were derived from global datasets, i.e. WATCH Forcing Data (WFD, Weedon *et al.*, 2010; 2011) and output from three GCMs for the A2 scenario, which has been made available through the EU-FP6 project WATCH (WATer and global CHange).

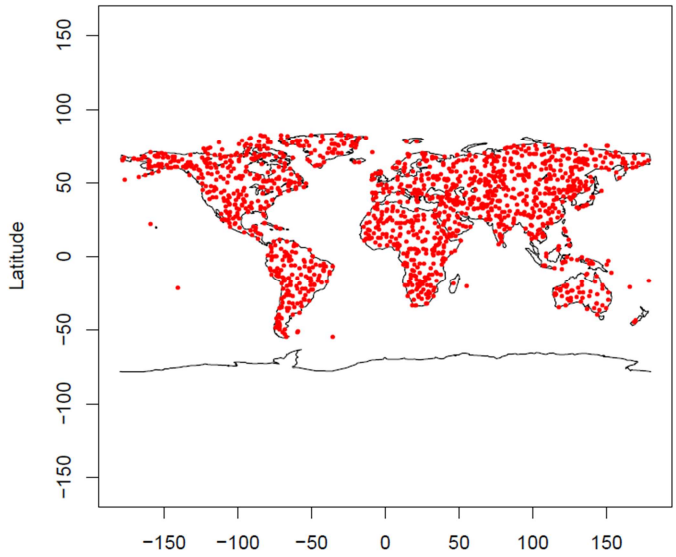

Figure 2.3 Selected land points (Melsen *et al.*, 2011).

Rainfall and snowfall data were added to obtain daily precipitation (Pra_t + Psn_t) for this study. The hydrological model determines on the basis of daily T_t retrieved from WFD, and *TT* according to the HBV approach (Section 2.1) if the precipitation is either rainfall or snow. Meteorological data (i.e. temperature, wind speed, altitude) were also retrieved to compute daily reference evaporation (ET_o) following the Penmann-Monteith equation (e.g. Allen *et al.*, 1998). WFD Radiation data were not used because of some inconsistencies among meteorological data at the daily time scale. Hence, the net radiation to compute ET_o was derived from WFD minimum en maximum temperature data and the latitude to compute extraterrestrial radiation (Allen *et al.*, 1998). WFD daily minimum en maximum temperature were computed by using the WFD 3-hourly temperature data.

Parameters to model snow accumulation and melt (Section 2.1) were chosen on the basis of experiences made by Seibert (2000; 2005). The threshold temperature *TT* was set at 0°C and the degree-day parameter *CFMAX* was assumed to equal 3.5 mm $^oC^{-1}$ day^{-1}, which reflects open landscape conditions. Snow losses (e.g. sublimation and undercatch) were supposed to be 20%, i.e. *CFCF*=0.8, and the melt water holding capacity (*CWH*) and the refreezing coefficient (*CFR*) were set as usually at 0.1 and 0.05, respectively.

Selection of land grid*s using the Köppen-Geiger hydroclimatic map*

In our controlled modeling experiment we have run the hydrological model not for all 67 420 land points that were distinguished for the WATCH study, but for a high number of randomly-selected land grids (Fig. 2.3), which are representative for the 5 Köppen-Geiger major climate types (Kottek *et al*., 2006). We selected 2% of all land grids, and to ensure that all 31 different Köppen-Geiger climate subtypes are well represented a stratified sample was defined meaning that from each of the climate subtypes 2% of land grids were selected with a minimum of 20 land grids. Table 2.2 gives the number of selected land grids per major climate type. In total we have selected 1495 land grids.

Table 1 Distribution of the selected land grids over the Köppen-Geiger climate types

Major climate type		Number
A	Equatorial climates	235
B	Arid climates	313
C	Warm temperate climates	242
D	Snow climates	506
E	Polar climates	199

Physical catchment structure

Land use was assumed to be a short vegetation with a rooting depth of 50 cm, which reflects permanent grassland. The soil information was derived from a standard series of soils that predominantly differ in soil texture (Wösten *et al.*, 2001). A mineral soil was chosen that consist of 30 cm topsoil overlying subsoil, which have different soil moisture retention characteristics. The selected moisture retention data result into a soil with a total available soil moisture of about 125 mm and readily available soil moisture of about 75 mm.

A groundwater system was defined through the response parameter *j* (Eq. 6). *j*=250 day was selected to represent an intermediary-responding groundwater system. This, for example, holds for a catchment with a transmissivity of 1000 m^2 d^{-1}, a storage coefficient of 0.1 and a stream distance of about 1.5 km. Readers are for more details referred to Van Lanen *et al*. (2011).

3. Results

Firstly we will describe the level of agreement between the high flow characteristics derived from the discharge obtained with the conceptual hydrological model using the re-analysis climate dataset (WFD) and those obtained with the climate datasets from the three GCMs for the control period (1971-2000). In the second part we will explain the high flow characteristics for the intermediate future (2021-2050) and for the end of the 21st Century (2071-2100), which are derived from the hydrological model driven by the climate dataset of the three GCMs (2001-2100).

3.1. High flows in the Control Period (1971-2000)

Time series of daily discharge have been simulated using the hydrological model (Section 2.1.2) for the period 1958-2001 using the WATCH Forcing Data (WFD) for the 1495 selected land grids. For each land grid the Q10 is determined for the control period (CTRL, 1971-2000). Daily discharge has also been simulated using the climate data from the three GCMs (ECHAM, CNRM and IPSL) for the period 1960-2100 (Section 2.3). This has been done for all 1495 land grids. For each land grid the Q10 is determined for the CTRL period. Probability distributions of Q10 for the different forcing datasets have been computed for each of five Köppen-Geiger major climate regions for the CTRL period (Fig. 3.1). Results are also plotted as Box-Whisker diagrams in Annex I.

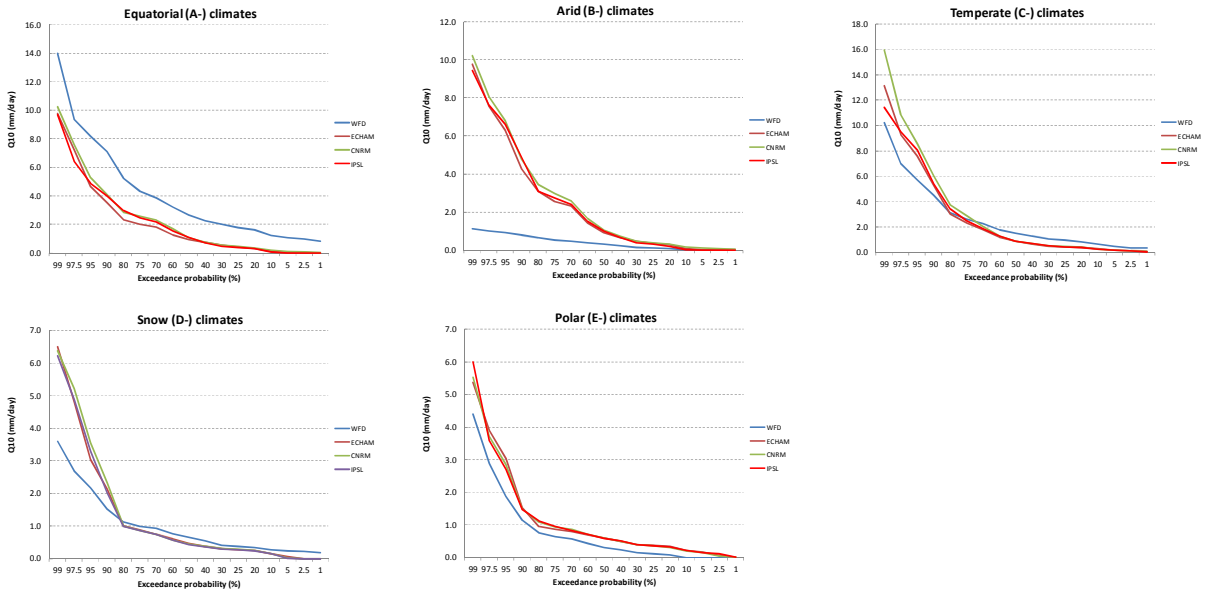

Figure 3.1 Probability distributions of the Q10 for different forcing dataset (WFD: re-analysis, and three GCMs: ECHAM, CNRM and IPSL) for the CRTL period (1971-2000). Distributions are presented for the five Köppen-Geiger major climate regions.

Figure 3.1 shows that the probability distributions of Q10 for the three GCMs are very similar, irrespective of the climate type, which means that the downscaled, bias-corrected climate data only slightly deviate. The largest differences among the GCMs are found in the tail of high Q10 for the temperate (C-) climate. Ideally the probability distributions of Q10 obtained with the GCMs should be equal to the distributions that are calculated using WFD, which would imply that the GCMs are able to capture historic climate. The distributions of Q10 for the temperate and polar climates (C- and E-climates) of the three GCMs have most in common with the WFD. The median of the Q10 of the three GCMs differs 40-42% and 89-94% for the C- and E-climates, respectively. The distribution of the Q10 for the WFD of the equatorial (A-) climate is higher than the three GCMs over the whole range of exceedance probabilities, which points at underestimation of the precipitation or overestimation of the

evapotranspiration by the GCMs. The median of the Q10 of the three GCMs deviates 59-64%. The Snow (D-) climate, but in particular the Arid (B-) climate are substantially different in the tail of high Q10. The median of the Q10 of the three GCMs differs 30-35% and 204-254% for the D- and B-climates, respectively.

The Box and Whisker plots (Annex I) also illustrate the higher median Q10 of the WFD than those of the GCMs for the Equatorial (A-) climate. The spread of the Q10 of the WFD is also higher. The Arid (B-) climate shows the opposite. The median of the Q10 and the spread of the WFD are clearly lower than those of the GCMs.

3.2. High flows in the 21st Century

The impact of climate change (A2-scenario) on high flows is presented in Figure 3.2. The impact is given as deviation of the median of the Q10 obtained from the hydrological model forced with the GCM climate data. This is done for the three GCMs (ECHAM, CNRM, IPSL) and for two periods (i.e. the intermediate future, 2021-2050, and the end of the 21st century, 2071-2100).

First, however, the Q10 obtained with the hydrological model forced with WFD is compared with the Q10 simulated with the hydrological model forced with each of the three GCMs for the control period (CTRL, 1971-2000). The results is presented as deviation (in %) of the WFD with the GCM, which was already introduced in Section 3.1. For three Köppen-Geiger major climate regions (A-, C- and D-climates) the deviation is negative implying that the Q10 obtained with the WFD forcing is smaller than the three Q10s with the GCM forcing. The opposite is found is for the B- and E-climate.

The impact of climate change according ECHAM and CNRM (Q10 as metric) is projected to increase over the 21st century for all five Köppen-Geiger major climate regions (Fig. 3.2). The projections according IPSL are more diffuse. For the C-, D- and E-climates the impact of climate change is expected to increase, similar as for ECHAM and CNRM. However, for the equatorial climate (A-climate) the IPSL projection points in the opposite direction, namely a decrease of the Q10. For the arid climate (B-climate) the impact is small, with a minor increase in the intermediate future and a decrease by the end of century.

The impact of climate change on the Q10 as projected with the three GCMs for the A2 scenario is most consistent for the temperate climate (C-climate, Fig. 3.2). The Q10 is expected to increase 8-10% in the near future (2021-2050) and 18-23% by the end of the century (2071-2100). The projected increase is lowest according to ECHAM. Please note that the differences for the control period between the reanalysis data (WFD) and the three GCMs are at least twice as high as the projected increase for the 21st century.

The expected impact of climate change on the Q10 according to the three GCMs for the A2 scenario is also rather consistent for the polar climate (E-climate, Fig. 3.2). The Q10 is projected to increase 10-16% in the near future (2021-2050) and 26-23% by the end of the century (2071-2100). The projected increase is lowest according to ECHAM. The increase is slightly higher than for the temperate climate, but the differences for the control period between the reanalysis data (WFD) and the three GCMs are also substantially larger than for the C-climate.

Two GCMs (i.e. CNRM and IPSL) are rather consistent in the expected impact of climate change on the Q10 (Fig. 3.2) for the cold climate (D-climate). The Q10 is projected to increase 15-17% in the near

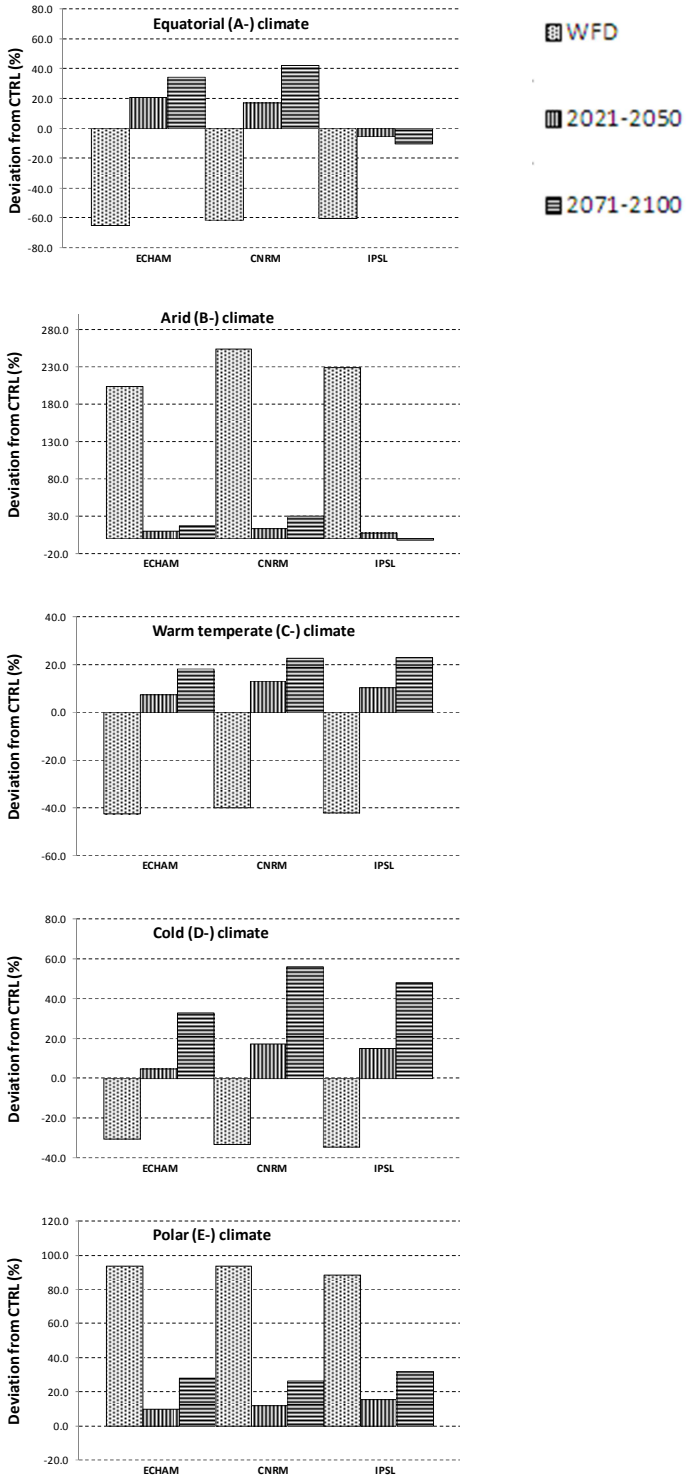

Figure 3.2 Deviation of the median of the Q10 from the WFD with the Q10 of the CTRL (1971-2000) for the three GCMs (WFD: 1st, 4th and 7th columns), and the deviation of the median of the Q10 from the three GCMs (ECHAM, CNRM or IPSL) for the A2 scenario with the Q10 of the CTRL for the intermediate future (2021-2050, 2nd, 5th and 8th column) and the end of the 21st century (2071-2100, 3rd, 6th and 9th column). Deviations are presented for the five Köppen-Geiger major climate regions.

future (2021-2050) and 48-56% by the end of the century (2071-2100). According to ECHAM the envisaged increase is lower, namely 5% in the near future and 33% by the end of the century. Increase of the Q10 by the end or the 21st century is similar to the differences for the control period between the reanalysis data (WFD) and the three GCMs.

The projected change of the Q10 due to climate change for the arid climate (B-climate) is significantly smaller than the differences for the control period between the reanalysis data (WFD) and the three GCMs (over 200%), as mentioned above. ECHAM and CNRM expect an increase of the Q10 of 10-16% in the near future (2021-2050) and 16-30% by the end of the century (2071-2100) (Fig. 2.3). IPSL envisages an increase of 8% in the near future, but a small decrease by the end of the 21st century (2%).

ECHAM and CNRM project an increase of the Q10 for the equatorial climate (A-climate) in the 21st century. The expected increase is 17-21% in the near future (2021-2050) and 35-42% by the end of the century (2071-2100) (Fig. 2.3). On the contrary IPSL expects a decrease of the Q10 by 6% in the near future and 10% by the end of the century. Similar as for the other climates, the change of the Q10m due to climate change is smaller than the differences between the reanalysis data (WFD) and the three GCMs for the control period.

4. Concluding remarks

The study on high flows with a conceptual hydrological model leads to the following conclusions for about 1500 randomly selected land points across the world that have an intermediate soil water supply capacity and an intermediary responding groundwater system:

- the probability distributions of Q10 (flow that is equalled or exceeded 10% of the time) for the three GCMs (ECHAM. CNRM, IPSL) are very similar for the control period (1971-2000), irrespective of the Köppen-Geiger climate type, which means that the downscaled, bias-corrected climate data from the climate models for the last part of the 20th century only slightly deviate;
- median Q10s derived from the GCMs for the CTRL period differ at least tens of per cent from the Q10 obtained when using WFD as input for the hydrological model (i.e. about 30-60%). The differences for the arid and polar (B- and E-) climates are higher because of the low discharge, and for the B-climate also due to overestimation of the high Q10s (about 100% or more);
- the impact of climate change (median of Q10 as metric) is projected to increase over the 21st century according to all three GCMs (A2 scenario) for the C-, D- and E-climates. This is also expected for the A- and B-climates according to ECHAM and CNRM. IPSL provides for these two Köppen-Geiger major climate regions a more diffuse projection;
- the projected increase of the median Q10 because of climate change (A2 scenario) varies between about 5 and 20% for the near future (2021-2050), irrespective of the Köppen-Geiger major climate region and the GCM. The only exception is IPSL that expects a decrease of the Q10 by about 5% for the equatorial climate;
- the projected increase of the median Q10 by the end of the 21st century (2071-2100) varies between about 15 and 60%,), irrespective of the Köppen-Geiger major climate region and the GCM. The only exception again is IPSL. This model expects a decrease of the median Q10 by about 2-10% for the equatorial and arid climates (A- and B-climates;
- difference between the median Q10 derived from the hydrological model forced with re-analysis data (WFD) and the same model forced with the down-scaled, bias corrected climate output from three climate models for the control period (1971-2000) clearly exceeds the differences found by climate change in the 21st century.

The analysis of high flows as obtained with the rather simple hydrological model in this study should be extended with:

- the outcome from the GCMs for the B1 scenario;
- an analysis at the global scale of the outcome from the suite of large-scale models that have been run within the WATCH project similar to the study of Miller et al. (2011) for Europe.

Acknowledgements

This research was undertaken as part of the European Union (FP6) funded Integrated Project 515 Water and Global Change (WATCH, contract 036946). The research is part of the programme of the Wageningen Institute for Environment and Climate Research (WIMEK-SENSE). The study contributes to the UNESCO IHP-VII programme (Cross-cutting programme FRIEND and Theme 1 Adapting to the impacts of global changes on river basins and aquifer systems)

References

Bates, B.C., Kundzewicz, Z.W., Wu, S. & Palutikof, J.P. (Eds.) (2008): Climate Change and Water. Technical Paper of the Intergovernmental Panel on Climate Change, IPCC Secretariat, Geneva, [available at: http://www.ipcc.ch/pdf/technical-papers/climate-change-water-en.pdf].

Birtles A.B. & Wilkinson, W.B. (1975): Mathematical simulation of groundwater abstraction from confined aquifers for river regulation. Water Resources Research 11(4): 571–580.

Bronswijk, J.J.B. (1988): Modelling of water balance, cracking and subsidence of clay soils, Journal of Hydrology 97(3-4): 199-212.

Chen, C., Hagemann, S., Clark, D., Folwell, S., Gosling, S., Haddeland, I., Hanasaki, N., Heinke, J. & Ludwig, F. and Voβ, F. (2011): Evaluation of projected hydrological changes in the 21st century obtained from a multi-model ensemble. WATCH Technical Report No. 45. [available at: http://www.eu-watch.org/publications/technical-reports]

EEA (2007): The pan-European environment: glimpses into an uncertain future. European Environmental Agency. EEA Report No 4/2007.

EEA (2008): Impacts of Europe's changing climate - 2008 indicator-based assessment. Joint EEA-JRC-WHO report, EEA Report No 4/2008, Copenhagen.

EEA (2010): Mapping the impacts of natural hazards and technological accidents in Europe. An overview of the last decade. EEA Technical report No 13/2010, Copenhagen, 2010.

Gudmundsson, L., Tallaksen, L.M., Stahl, S., Clark, D., Hagemann, S., Bertrand, N., Gerten, D., Hanasaki, N., Heinke, J., Voß, F. & Koirala, S. (submitted): Comparing Large-scale Hydrological Models to Observed Runoff Percentiles in Europe. (submitted to Water Resources Research).

Gudmundsson, L., Tallaksen, L.M. & Stahl, K. (2011): Projected changes in future runoff variability - a multi model analysis using the A2 emission scenario. WATCH Technical Report No 49 [available at: http://www.eu-watch.org/publications/technical-reports].

Haddeland, I., Clark, D., 560 Franssen, W., Ludwig, F., Voss, F., Arnell, N., Bertrand, N., Best, M., Folwell, S., Gerten, D., Gomes, S., Gosling, S. N., Hagemann, S., Hanasaki, N., Harding, R., Heinke, J., Kabat, P., Koirala, S., Oki, T., Polcher, J., Stacke, T., Viterbo, P., Weedon, G. P., and Yeh, P. (2011): Multi-model estimate of the global water balance: setup and first results, J. Hydrometeor., DOI:10.1175/2011JHM1324.1.

Hagemann, S., C. Chen, J.O. Haerter, J. Heinke, D. Gerten & C. Piani (2011): Impact of a statistical bias correction on the projected hydrological changes obtained from three GCMs and two hydrology models J. Hydrometeor. 12 (4), doi: 10.1175/2011JHM1336.1: 556-578.

Kraijenhof van de Leur, D.A. (1962): Some effects of the unsaturated zone on nonsteady free-surface groundwater flow as studied in a sealed granular model. Journal of Geophysics Research 67(11): 4347–4362.

Melsen, L.A., van Lanen, H.A.J. Wanders, N., van Huijgevoort, M.H.J. & Weedon, G.P. (2011): Reference evapotranspiration with radiation-based and temperature-based method - impact on hydrological drought using WATCH Forcing Data. WATCH Technical Report No. 39, 35 pg.

Miller, J., Kjeldsen, T. & Prudhomme, C. (2011): Assessment of Flood Peak Simulations by Global Hydrological Models. WATCH Technical Report No. 35.

Kottek, M., Grieser, J., Beck, C., Rudolf, B. & Rubel, F. (2006): World Map of the Köppen-Geiger climate classification updated. Meteorol. Z. 15: 259-263. DOI: 10.1127/0941-2948/2006/0130.

Piani C., J.O. Haerter & E. Coppola (2010a): Statistical bias correction for daily precipitation in regional climate models over Europe. Theor. Appl. Climatol., 99, 187–192, doi: 10.1007/S00704-009-0134-9.

Piani, C., G.P. Weedon, M. Best, S.M. Gomes, P. Viterbo, S. Hagemann, & J.O. Haerter, (2010b): Statistical bias correction of global simulated daily precipitation and temperature for the application of hydrological models. J. Hydrol., 395, 199-215, doi:10.1016/j.jhydrol.2010.10.024.

Prudhomme, C., Parry, S., Hannaford, J., Clark, D.B., Hagemann, S. & Voss, F. (2011) How well do large-scale models reproduce regional hydrological extremes in Europe? J Hydrometeo., doi: 10.1175/2011JHM1387.1.

Ritzema, H.P. (1994): Subsurface Flow to Drains. In: Ritzema, H.P (Ed.), Drainage Principles and Applications, 2nd edition, International Institute for Land Reclamation and Improvement, Wageningen, pg. 263-303.

Seibert, J. (2000): Multi-criteria calibration of a conceptual runoff model using a genetic algorithm. Hydrology and Earth System Sciences, 4(2): 215--224.

Seibert, J. (2005): HBV light version 2, user's manual. Retrieved March 24, 2009, from http://people.su.se/~jseib/HBV/HBV manual 2005.pdf.

Van Lanen, H.A.J. & Tallaksen, L.M. (2007): Hydrological drought, climate variability and change. In: Heinonen, M. (Ed.) Climate and Water. Proc. of the third Int. Conf. on Climate and Water, Helsinki, Finland, 3-6 September 2007, pg. 488-493.

Van Lanen, H.A.J., Weerts, A.H., Kroon, T. & Dijksma, R. (1996): Estimation of groundwater recharge in areas with deep groundwater tables using transient groundwater flow modelling. Proc. Int. Conf. on 'Calibration and Reliability of Groundwater Modelling', September 1996, Golden, USA, pp. 307 316.

Van Lanen, H.A.J., Fendeková, M., Kupczyk, E., Kasprzyk, A. & Pokojski, W. (2004): Flow Generating Processes, Chapter 3. In: Tallaksen, L.M. & van Lanen, H.A.J. (Eds.) (2004) Hydrological Drought. Processes and Estimation Methods for Streamflow and Groundwater. Developments in Water Science, 48, Elsevier Science B.V., pg. 53-96.

Van Lanen, H.A.J., Wanders, N., Tallaksen., L.M. & Van Loon, A.F. (2011): Hydrological drought across the world: impact of hydroclimatology and physical catchment structure. International Journal of Climatology (submitted).

Van Loon, A.F., van Lanen, H.A.J., Hisdal H., Tallaksen L.M., Fendeková, M., Oosterwijk, J., Horvát, O. & Machlica, A. (2010): Understanding hydrological winter drought in Europe. In: Servat, E., Demuth, S., Dezetter, A., Daniell, T., Ferrari, E., Ijjaali, M., Jabrane, R., van Lanen, H. & Huang, Y. (Eds.) Global Change: Facing Risks and Threats to Water Resources, IAHS Publ. No. 340, pg. 189-197.

Van Stiphout, T.P.J., van Lanen, H.A.J., Boersma, O.H. & Bouma, J. (1987): The effect of bypass flow and internal catchment of rain on the water regime in a clay loam grassland soil. J. of Hydrology 95 (1/2): 1 11.

Weedon, G.P., Gomes, S., Viterbo, P., Österle, H., Adam, J.C., Bellouin, N., Boucher, O., and Best, M., 2010. The WATCH forcing data 1958-2001: a meteorological forcing dataset for land surface- and hydrological-models., Tech. rep., WATCH Technical Report no. 22, available at: http://www.eu-watch.org/nl/25222760-Technical Reports.html.

Weedon, G., Gomes, S., Viterbo, P., Shuttleworth, J., Blyth, E., Sterle, H., Adam, J., Bellouin, N., Boucher, O.,and Best, M. (2011): Evidence of changing evaporation in the late twentieth century from the WATCH Forcing Dataset, J. Hydrometeorol., doi: 10.1175/2011JHM1369.1.

Wösten, J.H.M., Pachepsky, Ya.A. & Rawls, W.J. (2001): Pedotranfer functions: bridging the gap between available basic soil data and missing soil hydraulic characteristics. J. of Hydrology 251: 123-150.

Yevjevich, V. (1967): An objective approach to definition and investigations of continental hydrologic droughts. Hydrology Papers 23, Colorado State University, Fort Collins, USA.

Annex I Box and Whisker plots of the Q10 for different forcing dataset (WFD: re-analysis, and three GCMs: ECHAM, CRNM and IPSL) for the CRTL period (1971-2000). Distributions are presented for the five Köppen-Geiger major climate regions.

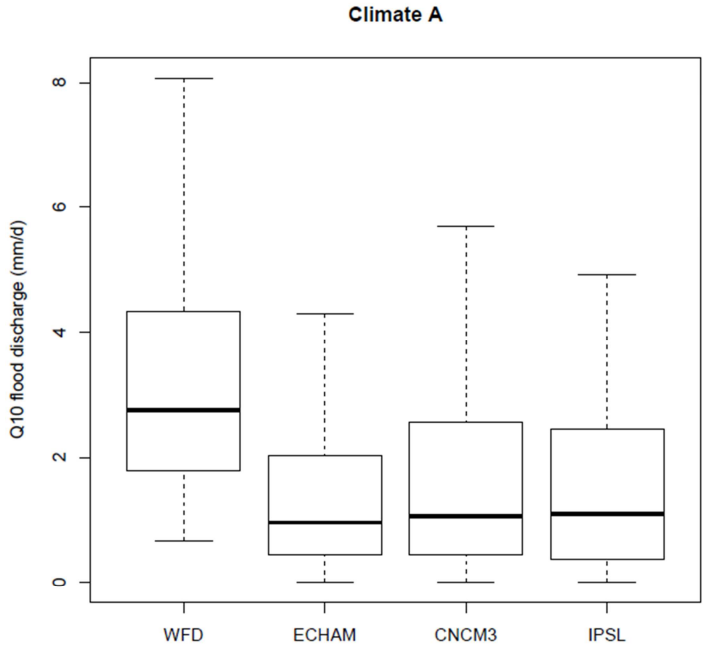

Figure IA Q10 for the Equatorial (A-) climate using different climate forcing (5, 25, 50, 75 and 90 quantiles).

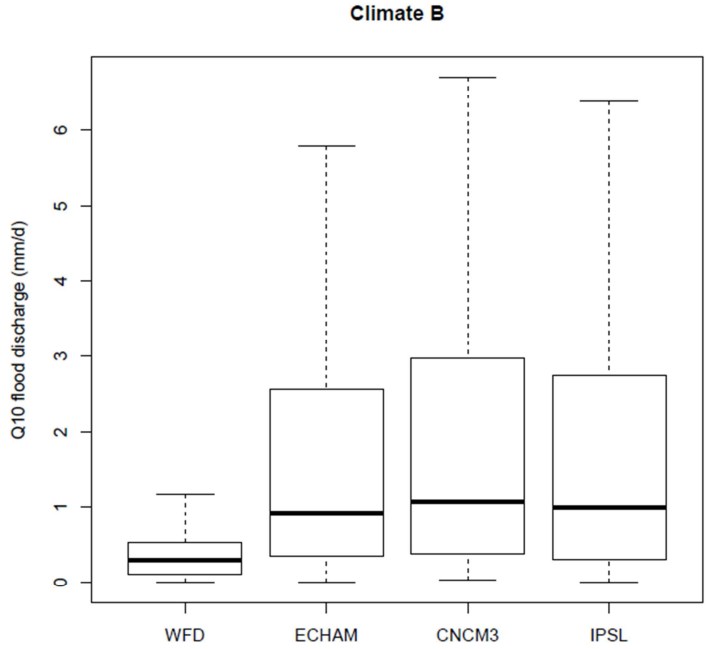

Figure IB Q10 for the Arid (B-) climate using different climate forcing (5, 25, 50, 75 and 90 quantiles).

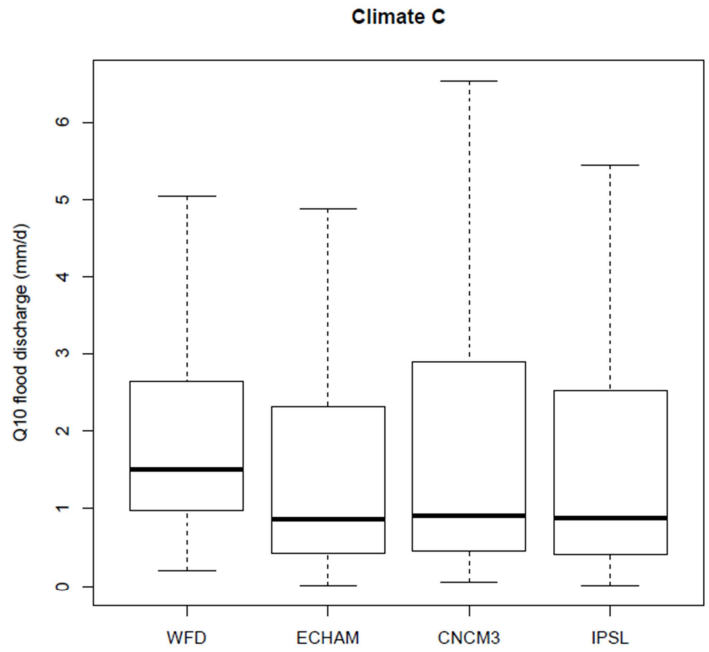

Figure IC Q10 for the Temperate (C-) climate using different climate forcing (5, 25, 50, 75 and 90 quantiles).

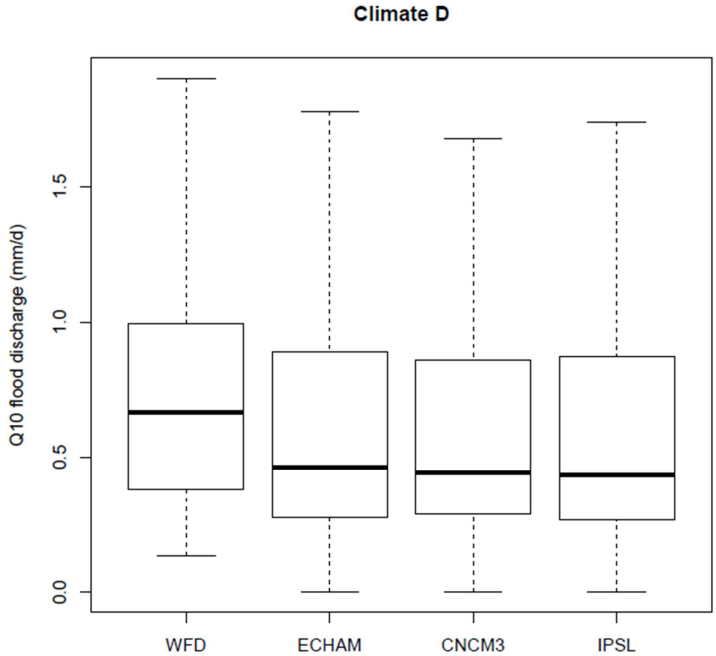

Figure ID Q10 for the Snow (D-) climate using different climate forcing (5, 25, 50, 75 and 90 quantiles).

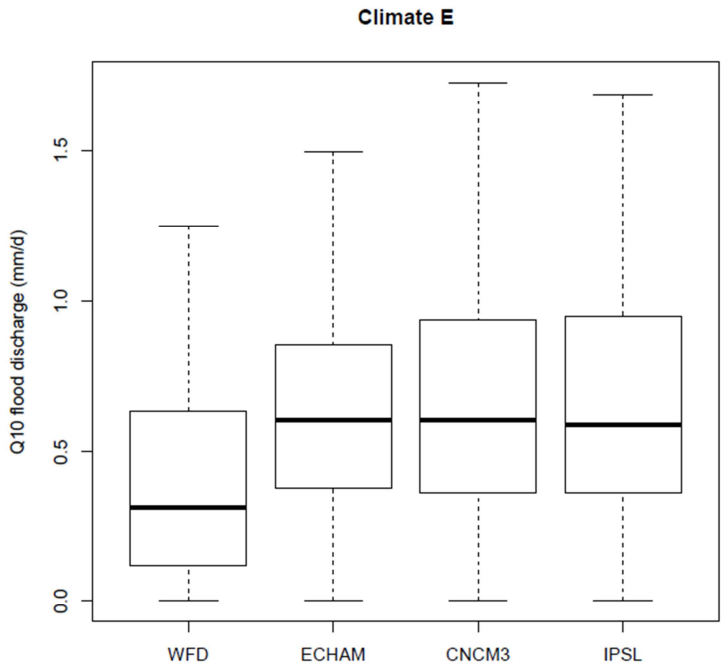

Figure IE Q10 for the Polar (E-) climate using different climate forcing (5, 25, 50, 75 and 90 quantiles).